Excitation of isovector giant resonances in pion single-charge exchange at 120, 165, and 230 MeV

F. Irom, J. D. Bowman, G. O. Bolme, E. Piasetzky,* and U. Sennhauser†
Los Alamos National Laboratory, Los Alamos, New Mexico 87545

J. Alster, J. Lichtenstadt, and M. Moinester
Raymond and Beverly Sackler Faculty of Exact Sciences, Tel Aviv University, Ramat-Aviv, Israel

J. N. Knudson‡
Arizona State University, Tempe, Arizona 85287

S. H. Rokni
Utah State University, Logan, Utah 84322

E. R. Siciliano‡
University of Georgia, Athens, Georgia 30602
and Los Alamos National Laboratory, Los Alamos, New Mexico 87545
(Received 28 August 1986)

We have measured doubly differential cross sections for the (π^+,π^0) and (π^-,π^0) reactions at 120- and 230-MeV kinetic energies for ^{40}Ca, ^{60}Ni, and ^{120}Sn. Nuclear-excitation energies up to 60 MeV were observed. We have extracted excitation energies, widths, and maximum cross sections for the isospin components of the isovector monopole resonance and the isovector dipole resonance. The excitation energies and widths from the present data and from earlier measurements at 165 MeV are compared and found to be in agreement. The cross sections for the isovector monopole and isovector dipole resonances show the same increase with bombarding energy in all targets. No isovector quadrupole strength is required to fit the experimental data. We compare the energy dependences of the isovector-resonance cross sections with those of isobaric-analog states, and to distorted-wave impulse approximation calculations.

We previously reported[1] on the study of isovector giant resonances in the pion charge-exchange reactions (π^+,π^0) and (π^-,π^0) at 165 MeV kinetic energy for targets from ^{40}Ca to ^{208}Pb. We determined the mass dependence of the cross sections, excitation energies, and widths for the $T+1$ and $T-1$ components of the isovector monopole resonance and isovector dipole resonance.

The object of the present work was to study these resonances at higher and lower energies, 230 and 120 MeV, for ^{40}Ca, ^{60}Ni, and ^{120}Sn. We sought to determine excitation energies and widths for the giant resonances at the different energies, to determine whether or not these quantities were independent of the bombarding energy. The energy independence of the excitation energies and widths is a test of the procedure used to separate the resonance peaks from the nonresonant background. We were also interested in comparing the energy dependence of the giant resonance cross sections to the energy dependence of isobaric-analog-state cross section, which are expected to be similar in the neighborhood of the (3,3) resonance. The energy dependence of the background cross section under the giant resonances was of additional concern: We wanted to find the bombarding energy at which the signal-to-background ratio was most favorable, in order to plane future study of isovector giant resonances.

The experiments were performed at the low-energy pion channel at the Clinton P. Anderson Meson Physics Facility (LAMPF). Typical pion fluxes were 10^7 π/s and typical momentum resolutions were less than 1%. Pion fluxes were determined by a scintillator-activation technique.[2] These measurements were frequently repeated to monitor possible changes in the pion flux. Outgoing π^0's were detected by the LAMPF π^0 spectrometer, which is described in Refs. 3 and 4. The energy and direction of the π^0's were reconstructed from the directions and energies of the two decay gammas using the formulas given in Ref. 3.

For our experiments the spectrometer was operated in its one-post configuration so that the scattering plane was horizontal. Three spectrometer settings (0°, 20°, and 37°) were used at 120 MeV and two settings (0° and 17°) were used at 230 MeV. The distances from the target to the first converter were 71 and 120 cm for the 120- and 230-MeV data, respectively. Target thicknesses were typically 1 g/cm^2. Runs with no target were taken to measure and correct for events occurring in the air between the end of the channel and the spectrometer. Random coincidences determined for out-of-time events were subtracted.

The energy and angular dependence of the acceptance of the spectrometer was determined by two methods. (1) The acceptance of the spectrometer was measured by observing yield from the reaction $\pi^-+p\rightarrow\pi^0+n$. The energy and angular dependence of the $\pi^-+p\rightarrow\pi^0+n$ cross section were obtained from the Arndt phase shifts solu-

tion.[5] At each spectrometer setting the yields from a CH_2 target were measured at the nominal beam energies (120 and 230 MeV) and at 20-MeV intervals below the beam energy. (2) The acceptance of the spectrometer was calculated using a Monte Carlo program that simulates experimental conditions. For energies above 100 meV and all scattering angles, the ratio of measured to calculated acceptance was found to be constant. For energies below 100 MeV the deviation between measured and calculated acceptance was considerably larger than could be attributed to uncertainties in the Monte Carlo program. We therefore attributed the variation in the ratio to uncertainties in the phase-shift solution. For energies below 100 MeV we took the acceptance of the spectrometer from the Monte Carlo calculations multiplied by the ratio of measured to calculated acceptance above 100 MeV. We will publish values for the $\pi^- + p \rightarrow \pi^0 + n$ cross sections in a future article.[6]

At each spectrometer setting the acceptance covers a 20° range of scattering angles. To obtain finer angular resolution, events were sorted, according to the reconstructed angle, into four angle bins per setting. The mean scattering angle and root-mean-square (rms) width for each bin were calculated using the Monte Carlo simulation program. The rms width was used to take into account the nonzero angular resolution of the spectrometer, using the approximate relation

$$\overline{d\sigma(\theta_i)/d\Omega} \simeq d\sigma(\theta_i)/d\Omega + \tfrac{1}{2}\sigma_i^2 \frac{\partial^2}{\partial\theta^2}[d\sigma(\theta_i)/d\Omega] ,$$

where $\overline{d\sigma(\theta_i)/d\Omega}$ Is the value of the differential cross section averaged over the acceptance of the ith bin, θ_i is the mean angle of the ith bin, and σ_i^2 is the mean square width of the ith bin. The above sorting procedures yielded doubly differential cross sections as functions of π^0 kinetic energy, T_{π^0}, for a number of forward scattering angles for each of the two bombarding energies. At 120 MeV the minimum and maximum bin angles were 5.7° and 46.3°; typical bin widths were 2.7° rms. At 230 MeV the minimum and maximum bin angles were 4.2° and 24.0°; typical bin widths were 2.0° rms.

The spectrometer settings and bins were chosen so that the fourth bin of one setting overlapped the first bin of the next. This allowed a direct means of normalizing the data taken at different spectrometer settings. The fluctuations in the normalization of the overlapped bins were 6% rms. By observing the fluctuations in the pion flux divided by the proton beam on the production target with the pion transport channel in a fixed condition, we determined that the reproducibility of the activation measurements of the pion flux is better than 2% rms. We therefore attribute the variation of the normalization factors to systematic errors in the Monte Carlo calculation of the spectrometer acceptance, and we assign a 4.3% ($6\%/\sqrt{2}$) systematic error to the bin-to-bin variation of the spectrometer acceptance.

In Figs. 1(a)–1(c) we show doubly differential cross-section data for the (π^-,π^0) reaction on ^{50}Ni at 120 and 230 MeV and for the (π^+,π^0) reaction at 230 MeV. Three angles are shown for each: (1) the most forward angle where the monopole and isobaric-analog-state peaks are large and the dipole peak is small, (2) an intermediate angle where the monopole and isobaric-analog-state peaks are small and the dipole peak is large, and (3) a large angle where all peaks are small.

The doubly differential cross sections were fitted to a phenomenological background function plus a sum of giant-resonance peaks. The background function was identical to that used in Ref. 1. In the fitting procedure the parameters in the background function were adjusted. The amplitude, width, and position (excitation energy) of each resonance and the amplitude and position of the isobaric-analog-state also were adjusted.

The basis for separating the giant-resonance peaks from the nonresonant background was the hypothesis that at fixed excitation energy the rate of change with momentum transfer squared, q^2 [$q = 2k\sin(\theta/2)$, where k is the momentum of the incident pion and θ is the scattering angle in the π-nucleus center of momentum], of the giant-resonance peaks, is much larger than the rate of change of the background. To demonstrate the validity of this hypothesis, we plot in Fig. 2 singly differential cross sections as functions of q^2, obtained by integrating the doubly differential cross sections over 10-MeV intervals. Three intervals were chosen at each bombarding energy: (1) one where the monopole peak is large, (2) one where the dipole peak is large, and (3) one where both resonances are small. For both bombarding energies the data from energy intervals where the giant resonances are small have a linear q^2 dependence. Figure 2 shows a linear function of q^2 fitted to the background interval data. The monopole and dipole interval data cannot be described as linear functions of q^2. The monopole interval cross sections decrease as q^2 is increased. The dipole interval cross sections increase and then decrease as q^2 is increased. These features of the data are the basis for the identification of monopole and dipole resonances. For the monopole and dipole intervals we show fits to the sum of a linear function of q^2 and the square of a Bessel function—$J_0^2(qR)$ for the monopole and $J_1^2(qR)$ for the dipole. The Bessel function form is expected for inelastic or charge-exchange reactions in the (3,3) resonance region, where the angular distributions are surface-related diffractive.[7]

In $T > 0$ nuclei, the $T_Z = T - 1$ components of the giant resonances excited in the (π^+,π^0) reaction are at higher excitation energies and have larger spreading and decay widths than those of the $T_Z = T + 1$ components excited in the (π^-,π^0) reaction. For the $T=0$ nucleus ^{40}Ca the cross section for the (π^-,π^0) reaction are larger than those for the (π^+,π^0) reaction. For the dipole state the ratio of the maximum π^- to maximum π^+ cross sections are consistent with the predictions of Auerbach based on the Coulomb polarization of the nuclear ground state.[8] For the monopole state the ratio of the maximum π^- to maximum π^+ cross sections are larger than those for the dipole state, but the errors in the ratios are also large. For the (π^+,π^0) data the giant-resonance signals were less distinct than those for the (π^-,π^0) data. The plots of energy-integrated cross sections versus q^2 do not show a clear resonance feature for the (π^+,π^0) data. The values of the resonance parameters that were extracted from a least squares fit to the (π^+,π^0) data have consistently larger errors than those assigned to those of the (π^-,π^0)

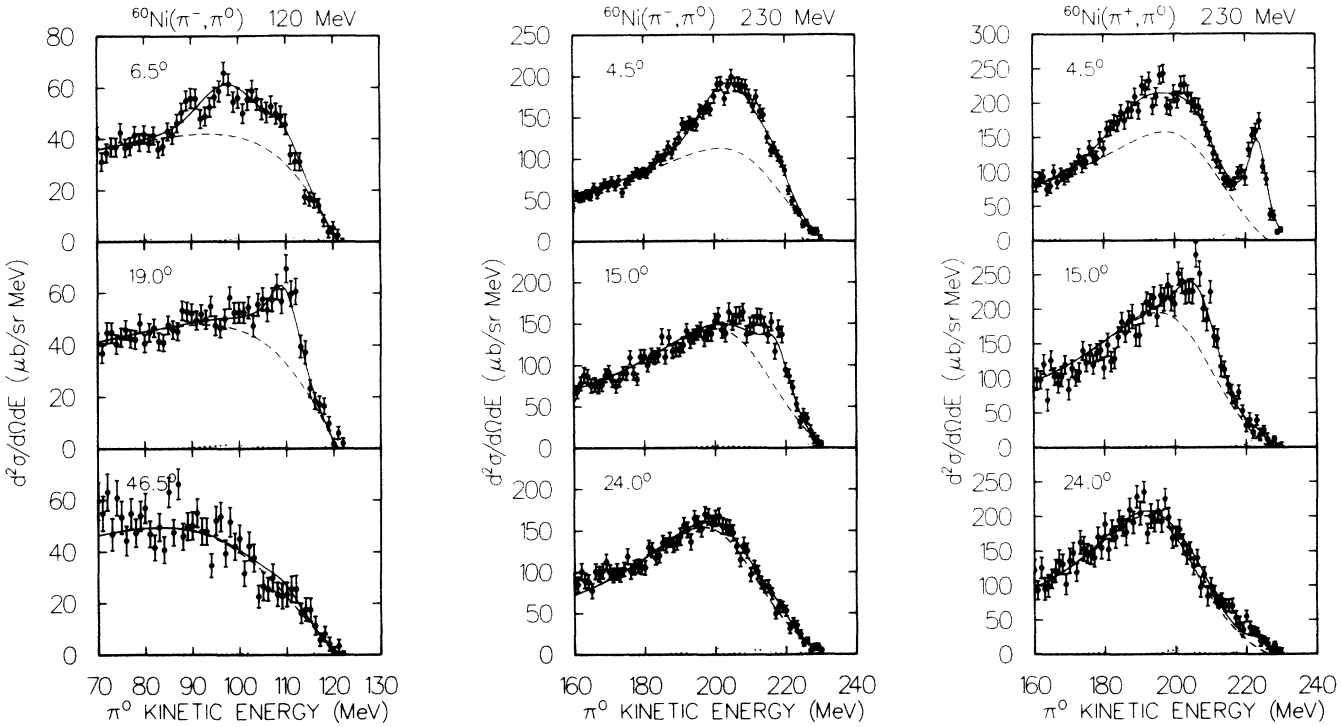

FIG. 1. Doubly differential cross sections for ^{60}Ni(π^-,π^0) reactions (a) and (b) at 120 and 230 MeV and for the ^{60}Ni(π^+,π^0) reaction (c) at 230 MeV. At each energy three angles are shown: top, a forward angle where the monopole (isobaric-analog-state) peak is large and the dipole peak is small; middle, an intermediate angle where the monopole peak is small and the dipole peak is large; and bottom, a large angle where both peaks are small. The solid curves are the fits to the data. The dotted curves represent the fitted decomposition into monopole, dipole, and isobaric-analog-state peaks for (π^+,π^0). The dashed curves represent the fitted background.

data. For more discussion of the differences between the (π^+,π^0) and (π^-,π^0) data, see Ref. 1.

The angular distributions used to extract the positions (excitation energies), widths, and cross sections of the resonance peak were calculated using a zero-range distorted-wave impulse approximation[9] (DWIA) and transition densities having Tassie forms.[10] Because higher-order dynamical processes are expected to be significant in the region of the (3,3) resonance, the DWIA is likely to be an incomplete model of the isovector π-nucleus reaction mechanism. Studies, however, have indicated that higher-order corrections to the DWIA tend to alter the absolute magnitude of the calculated cross sections without significantly affecting the shapes of the angular distribution. Thus, for the extraction of the differential isovector multipoles from the data, the DWIA shapes are expected to be reasonable. This expectation is justified in the resonance energy region and for forward scattering angles where the scattering is surface-related diffractive. In Fig. 3 we show representative DWIA angular distributions for the monopole, dipole, and quadrupole resonances at 230 MeV for the ^{60}Ni(π^-,π^0) reaction.

The reduced χ^2 values for the fits to the data were typically 1.2. The fitted background parameters for each target, projectile charge, and energy are given in Table I. The corresponding parameters at 165 MeV are given in Table IV of Ref. 1.

The excitation energies (relative to the target ground states), widths, and maximum cross sections extracted for the monopole and dipole resonances are given in Table II. The errors quoted are dominated in most cases by the arbitrary nature of the background function that was assumed. Had we assumed a different parametrization for the background function, which was constrained to be a slowly varying function of q^2 at each excitation energy, a comparable χ^2, but with slightly different values of the resonance parameter, would have resulted. We estimated these fitting errors by comparing the results for resonance parameters obtained using different assumptions concerning the nonresonant backgrounds as described in Ref. 1. The excitation energies, as well as the widths, at the three projectile energies are consistent. In Fig. 4 we plot the extracted excitation energies and widths of the resonances versus pion bombarding energy.

We also obtained maximum (0°) differential cross sections for the isobaric-analog states in ^{60}Ni and ^{120}Sn for the (π^+,π^0) reaction at 230 MeV. The 0° differential cross section for ^{60}Ni was 1.20±0.10 mb/sr; for ^{120}Sn it was 2.53±0.20 mb/sr. At 230 MeV, using the formula[11]

$$\frac{d\sigma}{d\Omega}=g(N-Z)/A^{\alpha},$$

with $g=26$ mb/sr and $\alpha=1.17$, which gives a good account of the systematics of the 0° cross section, we obtain

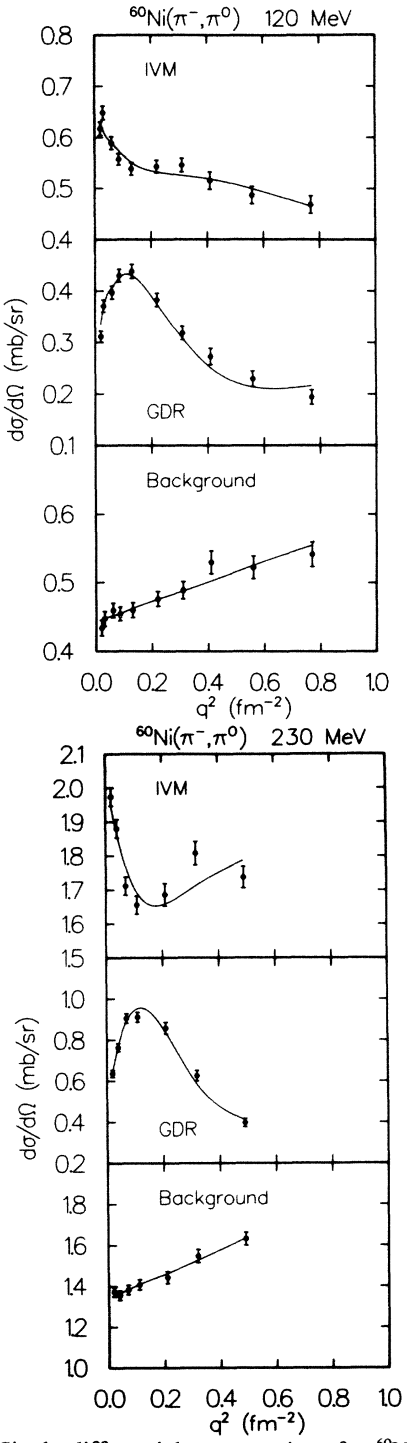

FIG. 2. Singly differential cross sections for ^{60}Ni(π^-,π^0) at (a) 120 MeV and (b) 230 MeV. The cross sections are as functions of q^2 obtained by integrating the doubly differential cross sections over 10-MeV intervals. Three intervals were chosen at each energy: top, one where the isovector monopole resonance (IVM) is large and intervals are centered at 29 MeV; middle, one where the giant dipole resonance (GDR) is large and intervals are centered at 11 MeV; and bottom, one where both resonances are small and intervals are centered at 44 MeV. The energy intervals refer to the corresponding abscissas in Fig. 1. For each plot we also show a fit to the sum of a linear function of q^2 and the square of a Bessel function—$J_0^2(qR)$ for the monopole and $J_1^2(qR)$ for the dipole (Ref. 7).

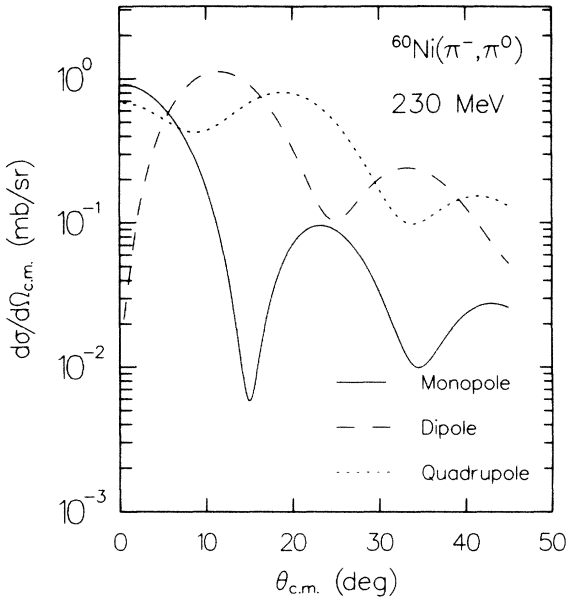

FIG. 3. Monopole, dipole, and quadrupole angular distributions calculated in the distorted-wave impulse approximation for the (π^-,π^0) reaction on ^{60}Ni at 230 MeV. These are the angular distributions used to fit the resonance peaks.

a value of 0.86 mb/sr for the ^{60}Ni cross section at 0° that is smaller than the measured value, 1.20±0.10 mb/sr. For ^{120}Sn the present value, 2.53±0.20 mb/sr, is consistent with the value of 2.10±0.25 mb/sr given in Ref. 11 and somewhat larger than the value predicted from the above formula, 1.92 mb/sr.

The maximum differential cross sections for monopole and dipole states quoted in Table II were obtained in fits where the width of each resonance varied at each of the three bombarding energies. To determine ratios of maximum differential cross sections at the three bombarding energies, we also performed fits at 120 and 230 MeV, where the width of each resonance was fixed to the values obtained at 165 MeV.[1] This procedure removed the statistical correlation between the maximum differential cross sections and the widths. The maximum differential cross sections for the monopole and dipole states from this analysis are shown in Fig. 5, plotted as a function of bombarding energy. The monopole and dipole maximum cross sections increase as the energy increases. The increase is similar from nucleus to nucleus for the two incident pion charges and for the monopole and dipole resonances.

The most complete experimental data for the 0° cross section of the isobaric-analog state in this mass and energy range are for ^{120}Sn and ^{60}Ni. These data are shown in Fig. 5. We also show the prediction of the fits to the systematic behavior of the isobaric-analog state using the formula given in Ref. 11. For ^{40}Ca we show the prediction from systematics for ^{42}Ca, for which an isobaric-analog state exists. For a strongly absorbed probe, such as the pion in the (3,3) resonance region, one expects surface-related diffractive scattering. Following the ideas developed in Ref. 9, it is possible to show that the energy dependences of the 0° cross section for the isobaric-analog

TABLE I. Parameters of the background functions described in Ref. 1 for ^{40}Ca, ^{60}Ni, and ^{120}Sn for two pion energies, 120 and 230 MeV. The value of the energy cutoff parameter T was found to be 900 MeV for all nuclei and both energies. The errors assigned to T are large and the results of the analysis depend weakly on the value of T.

Reaction	A_0	A_1	A_2	W_{L0}	α	E_0	g.s.
				120 MeV π^-			
^{40}Ca	0.63	6.21	−2.85	24.19	6.68	127.55	123.28
^{60}Ni	0.73	4.11	4.63	26.88	29.11	127.10	120.71
^{120}Sn	0.71	2.28	9.52	27.98	28.73	115.32	121.01
				120 MeV π^+			
^{40}Ca	0.86	4.97	−3.21	35.01	−8.44	126.70	111.48
				230 MeV π^-			
^{40}Ca	0.32	5.93	−13.97	23.71	−14.54	215.56	230.90
^{60}Ni	0.39	6.34	−15.27	24.80	−9.17	215.08	230.97
^{120}Sn	0.37	5.31	−11.48	23.99	3.89	214.57	231.51
				230 MeV π^+			
^{40}Ca	0.31	4.06	−10.56	24.86	−21.68	204.11	221.61
^{60}Ni	0.48	6.22	−17.27	24.90	−17.30	208.99	225.11
^{120}Sn	0.67	5.26	−16.90	21.59	−3.68	206.89	233.64

state, the monopole resonance, and the maximum cross section for the dipole resonance should all be approximately the same and should be proportional to

$$\frac{d\sigma}{d\Omega_{\max}} \sim \frac{d\sigma/d\Omega(\pi^- p \to \pi^0 n)}{d\sigma/d\Omega(\pi^- p \to \pi^- p) + d\sigma/d\Omega(\pi^+ p \to \pi^+ p)} k^2 .$$

We also plot this function in Fig. 5. The variation of the maximum cross sections of the monopole and dipole resonances with energy is similar to the above function. From 120 to 165 MeV the maximum cross section of the isobaric-analog state increases in the same way as the maximum cross sections for the monopole and dipole resonances increase. From 165 to 230 MeV the increase of the isobaric-analog-state maximum cross sections is less than those for the monopole and dipole resonances.

The volume integral of the transition density for the monopole resonance is zero. A positive transition density in the nuclear surface is cancelled by a negative value in the interior. At all three energies (120, 165, and 230 MeV) the classical pion mean free paths in nuclear matter are small (1.1, 0.6, and 0.8 fm, respectively) and the pion does not probe the nuclear interior. There is a negligible cancellation of positive scattering amplitude from the nuclear surface by negative scattering amplitude from the interior. The above cancellation therefore is not the explanation for differences between the energy dependences of monopole and isobaric-analog-state maximum cross sections. In fact, the above effect would lead to a decrease in the ratio of monopole to isobaric-analog-state maximum cross sections as the pion bombarding energy was either increased or decreased from 165 MeV, in contradiction to the observed behavior of the ratio.

In Fig. 6 we show the value of the fitted background (doubly differential cross section) at the energy of the monopole peak as a function of bombarding energy. The increase of the background cross section with bombarding energy is slower than that of the giant resonance cross sections between 165 and 230 MeV. This implies that, for fixed energy resolution, 230 MeV is the best of the three bombarding energies from the point of view of signal-to-background ratio. The improvement in the ratio of resonance cross section to background cross section between 120 and 230 MeV can be seen in Fig. 2 as well.

The forms $J_0^2(qR)$ and $J_1^2(qR)$ with $R = 1.37A^{1/3}$ fm are good approximations to the DWIA calculations for monopole and dipole states, respectively. Experimental data[12] for $\pi^{\pm}$ elastic-scattering angular distributions at 180 MeV from a wide range of nuclei can be described by the form $d\sigma/d\Omega \simeq J_1^2(qR)/(qR)^2$, where the strong-absorption radius is given by $R = 1.37A^{1/3}$. To test the suitability of the angular distributions for the giant resonances that we assumed in the extraction of the resonance parameter, we performed fits using the following forms for the angular distribution of the monopole and dipole states,

$$J_0^2[2kR \sin(\theta/2)] \text{ for the monopole}$$

and

$$J_1^2[2kR \sin(\theta/2)] \text{ for the dipole},$$

with R as a free parameter. As in Ref. 1 the fitted values of R agreed with $R = 1.37A^{1/3}$ within the 10% errors to which they were determined. The extracted resonance parameters obtained in this method (using Bessel functions for angular distribution) were the same as those extracted using the DWIA angular distributions to within a small fraction of the errors given in Table II. The position of the first minimum in the angular distribution of the monopole and dipole can be obtained from the fitted value of R from the relations

$$X_0^0 = 2kR \sin(\theta_{\min}/2) \text{ for the monopole}$$

TABLE II. Extracted excitation energies (relative to the target ground state), widths, and maximum cross sections for the isovector monopole (mono.) and isovector dipole (dip.) resonances for ^{40}Ca, ^{60}Ni, and ^{120}Sn at the three bombarding energies.

		120 MeV			165 MeV			230 MeV		
Reac.	Res.	Excitation energy (MeV)	Width (MeV)	Peak cross section (μb/sr)	Excitation energy (MeV)	Width (MeV)	Peak cross section (μb/sr)	Excitation energy (MeV)	Width (MeV)	Peak cross section (μb/sr)
^{40}Ca π^-	Mono.	27.0±2.0	16.1±3.6	341.0±100.0	24.1±1.5	21.6±1.9	768.0± 200.0	26.1±2.5	23.8 ±2.6	1881.0±380.0
	Dip.	14.6±1.5	6.8±1.3	464.0±100.0	13.8±1.6	5.7±2.3	856.0± 87.0	14.9±1.5	6.2 ±0.9	1481.0± 80.0
^{40}Ca π^+	Mono.	33.7±2.0	14.3±3.2	234.0± 70.0	35.9±2.9	24.2±4.0	533.0± 220.0	38.1±3.3	24.5 ±3.6	984.0±300.0
	Dip.	25.9±1.5	6.8±1.0	454.0± 46.0	24.7±2.1	6.4±1.9	725.0± 126.0	26.1±1.5	8.1 ±1.0	1214.0±100.0
^{60}Ni π^-	Mono.	23.2±1.7	13.9±2.3	279.0± 90.0	25.2±1.7	14.7±2.1	725.0± 185.0	25.2±1.9	18.1 ±1.5	1929.0±200.0
	Dip.	12.4±1.5	6.7±1.5	386.0± 50.0	13.5±1.6	4.2±2.0	358.0± 75.0	13.7±1.5	6.9 ±1.3	856.0±100.0
^{60}Ni π^+	Mono.				35.6±2.8	18.4±4.1	704.0± 280.0	36.6±2.5	23.1±2.0	1609.0±500.0
	Dip.				25.3±1.5	6.4±1.7	792.0± 190.0	24.0±1.5	10.2±1.4	2028.0±200.0
^{120}Sn π^-	Mono.	20.6±1.5	5.3±2.9	242.0± 50.0	21.4±2.2	9.2±2.6	532.0± 108.0	21.3±1.7	9.9±1.3	1164.0±180.0
	Dip.				9.6±1.8	(0)[a]	193.0± 46.0			
^{120}Sn π^+	Mono.				30.0±3.0	1.60±4.1	1277.0±1110.0	31.9±2.5	16.2±4.6	1618.0±604.0
	Dip.				23.9±0.9	3.4±2.1	858.0± 335.0	22.9±1.5	5.4±1.8	2039.0±260.0

[a]The width of the ^{120}Sn $T+1$ dipole was fixed to 0 in the fits; see Ref. 1.

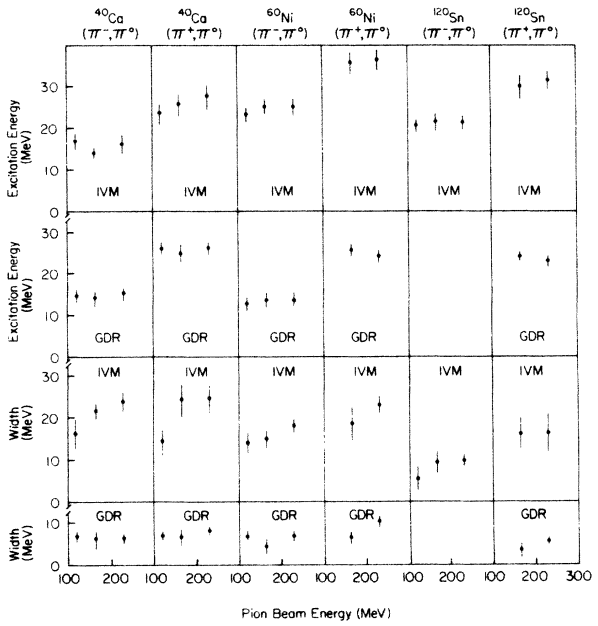

FIG. 4. Extracted excitation energies and widths for ^{40}Ca, ^{60}Ni, and ^{120}Sn($\pi^{\pm},\pi^0$) reactions for the isovector monopole resonances (IVM's) and giant dipole resonances (GDR's) plotted versus the pion bombarding energy.

and

$$X_0^1 = 2kR \sin(\theta_{\min}/2) \text{ for the dipole ,}$$

where $X_0^0 = 2.40$ is the first zero of $J_0(X)$ and $X_0^1 = 3.83$ is the second zero of $J_1(X)$. In Fig. 7 we plot values for $\theta_{\min}$ for the monopole and dipole resonances excited in the (π^-,π^0) reaction for ^{60}Ni as functions of the inverse of the momentum of the incident pion. The figure shows that the monopole and dipole angular distributions shift to more-forward angles as the incident pion momentum increases. The solid lines shown in Fig. 7 represent the prediction of the above relations for $\theta_{\min}$ with $R = 1.37A^{1/3}$. The angular distributions for the monopole and dipole shift forward in the way expected from surface-related diffractive scattering with a constant interaction radius.

As in Ref. 1 no isovector quadrupole peak was required to fit the data, although the range of scattering angles extends beyond the second maximum of the quadrupole angular distribution. In order to quantify the absence of the isovector quadrupole resonance, we performed fits to the (π^-,π^0) data in which the amplitudes of isovector quadrupole peaks were allowed to vary. The excitation energies and widths of the quadrupole peaks are taken from the random-phase approximation (RPA) calculations of Ref. 13 (method IV). This calculation predicts that the

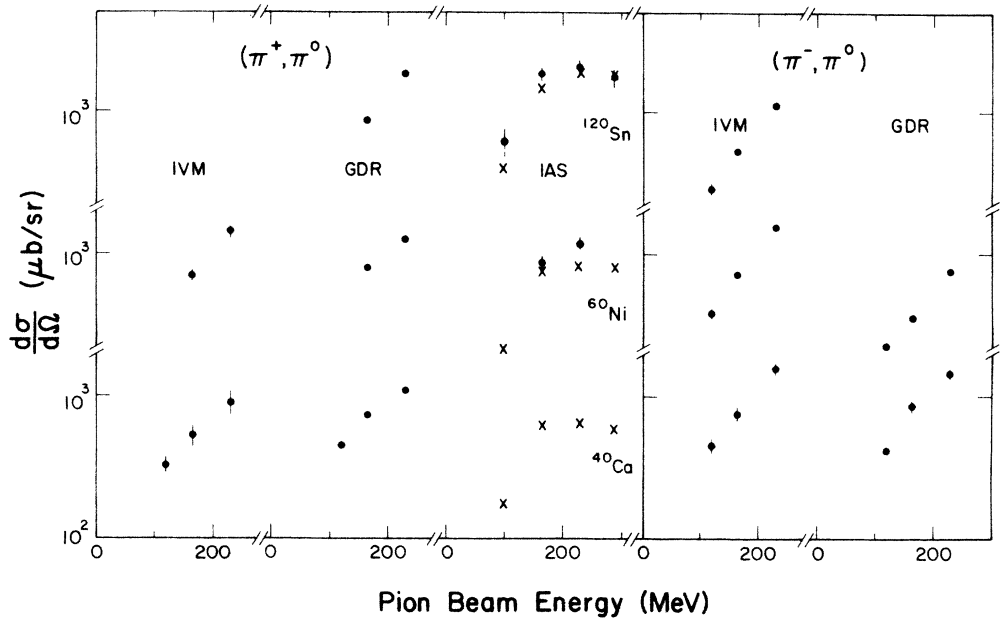

FIG. 5. Maximum cross sections for (π^+,π^0) and (π^-,π^0) for the isovector monopole resonances, giant dipole resonances, and isobaric-analog states as a function of bombarding energy. For ^{60}Ni and ^{120}Sn we plot experimental results of the 0° cross sections for the isobaric-analog state (IAS) from this work and Ref. 11 (solid circles). We also plot the expected values from systematics of the isobaric-analog state using the formula given in Ref. 11 (solid symbols). For ^{40}Ca there is no isobaric-analog state and we plot the expected values from systematics of the isobaric-analog state for ^{42}Ca (crosses). We also show the energy dependence of the maximum cross sections for the monopole, dipole, and isobaric-analog state using the approximate expression discussed in the text (solid curve). The energy dependence for the monopole and dipole maximum cross sections are similar and they are the same as the energy dependence of the approximate expression (solid curve). The isobaric-analog state maximum cross section increases less than the resonances cross sections from 165 to 230 MeV.

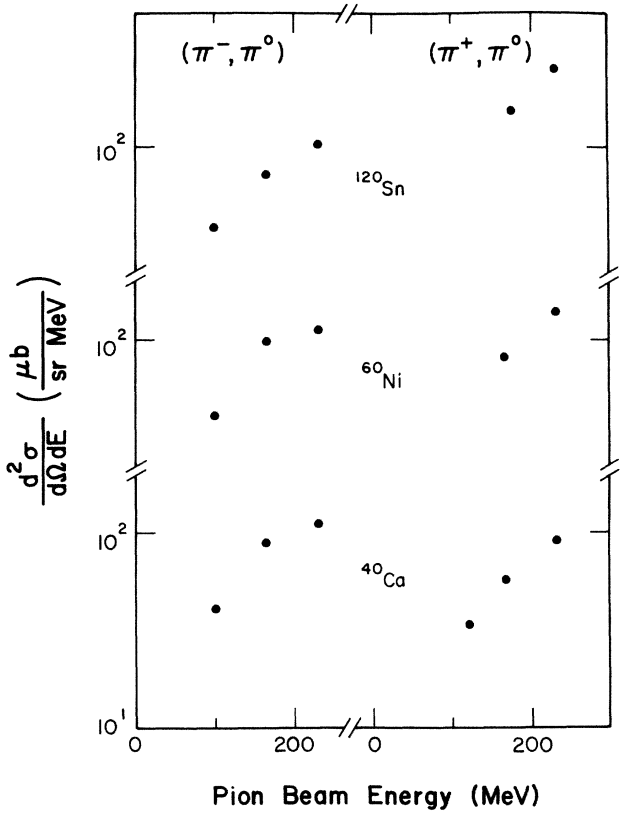

FIG. 6. Doubly differential cross sections for the fitted background at the energy of the isovector monopole resonances as a function of the pion bombarding energy.

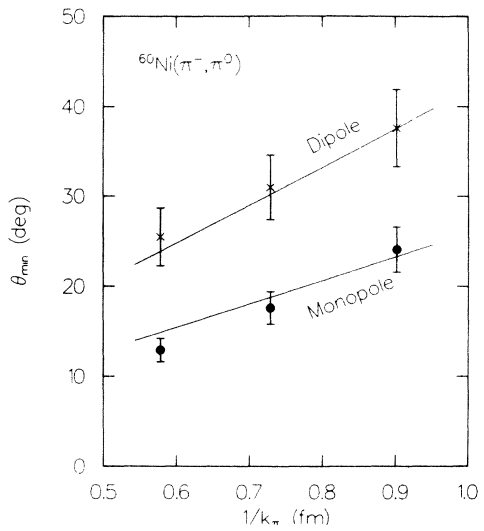

FIG. 7. Location of the first minimum of the isovector monopole resonance and the second minimum of the isovector giant dipole resonances excited by the (π^-,π^0) reaction on ^{60}Ni vs the inverse of the momentum of the incident pions. The solid lines represent the prediction for the location of the minima for a constant interaction radius $R=1.37A^{1/3}$ fm (see text).

excitation energy of the isovector quadrupole should be close to that of the monopole and that the quadrupole width is somewhat narrower than that of the monopole. The shapes of the angular distributions were taken from DWIA calculations described above. When the amplitude of a possible quadrupole peak was allowed to vary, the ex-

TABLE III. Isovector quadrupole results. The first two rows give the excitation energies and widths assumed in the extraction of the differential cross section at the second maximum of the isovector quadrupole peak at each bombarding energy. At each of the three energies we also compare the maximum cross section with the results of zero-range RPA-DWIA calculations. The corresponding average ratio for the isovector monopole and dipole resonances is 0.67.

	^{40}Ca	^{60}Ni	^{120}Sn
Quadrupole excitation			
Energy (MeV)	26.4	25.1	19.3
Width (MeV)	10	7	4
120 MeV			
second maximum cross sections (μb/sr)	175±140	38±80	61±40
RPA-DWIA (μb/sr)	286	202	137
Ratio	0.61±0.49	0.19±0.40	0.45±0.29
165 MeV			
second maximum cross sections (μb/sr)	23±60	0±80	1±50
RPA-DWIA (μb/sr)	728	482	297
Ratio	0.03±0.08	0.00±0.17	0.00±0.17
230 MeV			
second maximum cross section (μb/sr)	234±300	190±240	300±200
RPA-DWIA (μb/sr)	1201	801	505
Ratio	0.19±0.25	0.24±0.30	0.59±0.40

citation energies, widths, and cross sections extracted for the monopole and dipole peaks were consistent with the values given in Table II to within the quoted errors. In Table III we give the values extracted for the isovector quadrupole cross section at the second maximum. The ratio of measured monopole and dipole cross sections to the RPA-DWIA calculations is 0.67. The ratio of measured quadrupole cross section to the RPA-DWIA calculation is considerably smaller.

In Ref. 1 and in the present work, we carried out a number of measurements to determine whether or not the features in the data we identified as the nuclear isovector monopole and dipole resonances have the properties expected for a nuclear giant resonance. Any state found in the charge-exchange reaction is an isovector state. The assignment of zero for angular momentum of the monopole state is made on the basis of the characteristic forward peaking of its angular distributions. The dipole state angular distribution has an $L=1$ shape. The strong-interaction radii for the monopole and dipole states extracted in a Bessel-function analysis agree with those found in elastic pion scattering. The angular distribution for the monopole and dipole states shifts forward in angle as the momentum of the incident pion is increased, as expected for surface-related diffractive scattering with constant strong interaction radius. In Ref. 1 we studied the variations of excitation energy, width, and maximum cross section with atomic mass at fixed pion energy; in the present work we studied the variation of excitation energy, width, and maximum cross section with bombarding energy for a few targets. The excitation energy and width of the states have a smooth dependence on the mass of the target and are in agreement with RPA calculations. Furthermore, they do not change when the bombarding energy is changed, providing a test of the analysis procedure. The cross sections of the states exhaust approximately 0.7 of the RPA-DWIA calculations. The maximum cross section for the monopole peak changes with energy in the same way as the maximum cross section for the dipole peak changes and in the way expected for surface-related diffractive scattering of resonance energy pions. The energy dependence of the background and the isobaric-analog-state cross sections was similar. Between 165 and 230 MeV both increased less than the resonance cross sections. We found much less isovector quadrupole strength than expected from RPA-DWIA calculations, and much less strength than displayed in our observations of the isovector monopole and dipole resonance.

ACKNOWLEDGMENTS

We thank the technical staff at LAMPF for their work in setting up the experimental apparatus and channel, and we acknowledge beneficial discussions with N. Auerbach and M. B. Johnson. This work was supported by the U.S. Department of Energy, the U.S.-Israel Binational Science Foundation, and National Science Foundation.

*Present address: Tel Aviv University, Tel Aviv 69978, Israel.
†Present address: SIN, Swiss Institute for Nuclear Research, CH-5234 Villigen, Switzerland.
‡Present address: Los Alamos National Laboratory, Los Alamos, NM 87545.

[1]A. Erell, J. Alster, J. Lichtenstadt, M. A. Moinester, J. D. Bowman, M. D. Cooper, F. Irom, H. S. Matis, E. Piasetzky, and U. Sennhauser, Phys. Rev. C **34**, 1822 (1986).
[2]B. J. Dropesky, G. W. Butler, C. J. Orth, R. A. Williams, M. A. Yates-Williams, G. Friedlander, and S. B. Kauffman, Phys. Rev. C **20**, 1814 (1979).
[3]H. W. Baer, R. D. Bolton, J. D. Bowman, M. D. Cooper, F. H. Cverna, R. H. Heffner, C. M. Hoffman, N. S. P. King, J. Piffaretti, J. Alster, A. Doron, S. Gilad, M. A. Moinester, P. R. Bevington, and E. Winkelmann, Nucl. Instrum. Methods **180**, 445 (1981).
[4]S. Gilad, Ph.D. thesis, Tel Aviv University, 1979.
[5]R. A. Arndt, Computer program SAID (Scattering Analysis Interactive Dial-in), Virginia Polytechnic Institute and State University, 1984.
[6]F. Irom, J. D. Bowman, H. W. Baer, E. Piasetzky, J. Alster, and M. A. Moinester, Phys. Rev. C (to be published).
[7]J. D. Bowman, M. B. Johnson, and J. W. Negele, Phys. Rev. Lett. **46**, 1614 (1981).
[8]N. Auerbach, Phys. Rev. Lett. **49**, 1376 (1982).
[9]N. Auerbach, M. B. Johnson, A. Klein, and E. R. Siciliano, Phys. Rev. C **29**, 526 (1984).
[10]L. J. Tassie, Aust. J. Phys. **9**, 407 (1956).
[11]U. Sennhauser, E. Piasetzky, H. W. Baer, J. D. Bowman, M. D. Cooper, H. S. Matis, H. J. Ziock, J. Alster, A. Erell, M. A. Moinester, and F. Irom, Phys. Rev. Lett. **51**, 1324 (1983).
[12]R. Corfu *et al.*, in *Meson-Nuclear Physics—1979 (Houston)*, proceedings of the 2nd International Topical Conference on Meson-Nuclear Physics, AIP Conf. Proc. No. 54, edited by E. V. Hungerford III (AIP, New York, 1979); R. A. Eisenstein, *ibid.*
[13]N. Auerbach and A. Klein, Phys. Rev. C **28**, 2075 (1983).